A Highly Luminous Sky-Blue Organic Light Emitting Diodes Based on the Bis-[(1,2)(5,6)]Indoloanthracene Emissive Layer

Khrystyna Ivaniuk[1], Vladyslav Cherpak[1], Pavlo Stakhira[1], Zenon Hotra[1,2], Boris Minaev[3], Gleb Baryshnikov,[3,4] Evgeniy Stromylo[3], Dmytro Volyniuk[5], Juozas V. Grazulevicius[5], Algirdas Lazauskas[6], Sigitas Tamulevicius[6], Bernhard Witulski[7], Mark E. Light[8], Pawel Gawrys,[8] Richard J. Whitby[8]**, Gabriela Wiosna-Salyga[9], Beata Luszczynska[9]*

[1] Lviv Polytechnic National University, S. Bandera 12, 79013 Lviv, Ukraine

[2] Rzeszów University of Technology, W. Pola 2, Rzeszów 35-959, Poland

[3] Bohdan Khmelnytsky National University, Shevchenko 81, 18031 Cherkassy, Ukraine

[4] Division of Theoretical Chemistry and Biology, School of Biotechnology, KTH Royal Institute of Technology, 10691 Stockholm, Sweden

[5] Department of Polymer Chemistry and Technology, Kaunas University of Technology, Radvilenu Plentas 19, LT-50254 Kaunas, Lithuania

[6] Institute of Materials Science, Kaunas University of Technology, Baršausko str. 59, LT-51423 Kaunas, Lithuania

[7] Laboratoire de Chimie Moléculaire et Thioorganique, UMR 6507 CNRS, ENSICAEN & University of Caen, 6 Bvd du Marechal Juin, 14050 Caen, France;

[8] Chemistry, University of Southampton, Southampton, HANTS, SO17 1BJ, U.K.

[9] Department of Molecular Physics, Lodz University of Technology, Zeromskiego str.116, 90-924 Lodz, Poland

ABSTRACT: An in-depth analysis of the electro-optical and light emissive properties was carried out with a new fused heteroacene, the bis [(1,2)(5,6)] indoloanthracene. The compound was synthesized in a straightforward bidirectional manner from 1,4-dibromo-2,5-diodobenzene utilizing a reaction cascade of isomerisation and cyclisation sequences. Bis-[(1,2)(5,6)] indoloanthracene exhibits bright luminescence with high quantum yield in solution as well as in the solid state. By using this novel semiconductor as active layer, an efficient OLED has been fabricated for which its emission pattern resembles at least two emitters in a single emissive region originated from the same molecule. One has its origin from the single molecule and is similar to the luminescence spectra in solution, whereas the other functions through the formation of aggregates being similar with the emission pattern found with crystals of bis-[(1,2)(5,6)]indoloanthracene. As a result bright sky-blue OLEDs with very high luminance exceeding 10000 cd/m^2 were obtained. Such color pattern and performance has not previously been observed with low molecular weight, electron-rich fused polycyclic aromatic compounds and indicate a promising new class of materials for development.

INTRODUCTION

The useful optoelectronic properties of organic π-conjugated molecules determine their widespread application in order to create efficient organic field effect transistors and highly luminous organic light emitting diodes (OLEDs)[1]. OLEDs are arguably the most promising branch of devices based on organic electronics. Indeed, after solving the problem of designing stable blue emitter prototypes applications have emerged and became available on the market within display products (smartphones, tablets TV sets) as well as OLED lightning devices.[1]

The overwhelming proportion of materials used in OLEDs are metal complexes, oligomers and polymers containing various amounts of aromatic and pi-conjugated units.[2, 3, 4, 5] Notably, charge transport and luminescent properties of solid-state organic semiconductors are determined by molecular structure and intermolecular interactions through either a short distance or a long range

periodical molecular-packing motif.[6] As a result, the flat structure of π-extended aromatic or heteroaromatic molecules often favor a molecular packing motif in the solid allowing also an efficient charge carrier transport through the spatial electronic delocalization in the constituent molecular building blocks.[7] Furthermore, the inherent rigidity of fused aromatic molecular units provide strong fluorescence properties in many cases.[8]

Particular electron-rich analogues of pentacene, namely indolocarbazoles, are currently investigated here. Certain layers of indolocarbazoles with long alkyl or alkylaryl chains exhibit a useful hole carrier mobility due to a favorable supramolecular organization in the solid state.[9] Notably, packing motif and performance of these indolocarbazoles can be altered by the chain length of attached alkyl moieties.[10] Moreover, non-symmetrical analogues of indolocarbazoles show appreciable performances[11], and the attachment of aryl groups on indolocarbazole nitrogens furthermore provided materials suitable for OLED applications.[12] Tuning of indolocarbazole properties may be performed through a formal extension of the π-conjugation by attaching aromatic moieties to the basic polycyclic frame.[13, 14, 15, 16, 17, 18] Finally, indolocarbazoles have been used as monomer units in either homo-[19, 20] or copolymers – the latter used as active components in FETs[21, 22] or OPVs.[23, 24, 25, 26, 27, 28]

Reports on more π-extended polycyclic aromatic compounds bearing carbazole units are less frequent.[29 , 30, 31] Impressive examples of π-extended heteroacenes show that polycyclic aromatic and heteroaromatic compounds are good candidates for transistors[32, 33, 34, 35, 36, 37, 38] , OLED[39, 40, 41] and OPV[42, 43] fabrications.

We believe that angularly fused acenes and heteroacenes with highly extended π-conjugation provide an important class of materials for applications in organic electronics. The angular fusion or heteroatom inclusion avoids the rapid onset of instability with increased length observed with linear acenes. The extended conjugation provides a useful way to fine–tune HOMO-LUMO band gaps and levels, as well as potentially providing greater opportunity for intermolecular π-system overlap.

In this paper we present experimental and theoretical data on the structure, photophysical properties including solution, solid state and film luminescence and charge carrier transport

properties of the novel sky-blue-emitting bis[(1,2)(5,6)]indoloanthracene (**4**) – a stable π-extended heteroacene.

EXPERIMENTAL METHODS

Luminescence spectra and luminescence decay curves of vacuum deposited layers of **4** and its chlorobenzene solution were recorded with the Edinburgh Instruments FLS980 spectrometer at room temperature using EPLED 340 nm picosecond pulsed light emitting diode as the excitation source.

UV absorption spectra in solution were recorded with a JASCO V-660 spectrometer and emission spectra with a Perkin Elmer LS55 fluorescence spectrometer. Absolute photoluminescence quantum yields as well as luminescence spectra of solids and in solution were recorded with the Hamamatsu CC9920 integration sphere set-up at room temperature. For quantum yield measurements solutions of **4** were purged with argon prior to measurement. Electrochemical studies were carried out at room temperature using a GAMRY Ref600 potentiostat. The working electrode was a platinum electrode, the auxiliary electrode a platinum wire. The reference electrode was an aqueous saturated (KCl) calomel electrode. Under the conditions used, the reversible potential for the ferrocenium/ferrocene couple at 298 K is +0.46 V in CH_2Cl_2. Solutions of **4** ($0.5x10^{-4}$M) in a $1x10^{-1}$ M Bu_4NPF_6 /CH_2Cl_2 electrolyte solution were used. TGA measurements were recorded on a Perkin Elmer Thermogravimetric Analyser TGA7.

The ionization potential (IP) of the layers of **4** was measured by the electron photoemission method in the air.[44] The samples were fabricated by means of vacuum deposition of compound **4** onto indium tin oxide (ITO) coated glass substrate. The experimental setup consisted of the deep-UV deuterium light source ASBN-D130-CM, the CM110 1/8m monochromator, and the 6517B Keithley electrometer.

To investigate the charge-mobility properties of the studied compounds we used the time-of-flight (TOF) method.[1] To construct samples for TOF measuring, the vacuum deposited layers of **4** onto ITO-coated glass substrate were completed by evaporated aluminum (Al) top-contacts. Individual

samples had areas of 0.06 cm^2. For TOF measurements a pulsed third-harmonic Nd:YAG laser (EKSPLA NL300) working at a pulse duration of 3-6 ns and wavelength of 355 nm was used to excite layers through the ITO glass. The 6517B Keithley electrometer was used to apply direct positive voltage to the ITO. The TOF signal was recorded by a digital storage oscilloscope Tektronix TDS 3032C.

To investigate photoluminescence and X-ray diffraction properties of **4** in solid state, thin layers of **4** were deposited onto pre-cleaned quartz substrates. Room temperature photoluminescence (PL) spectra of the layers of **4** were investigated using a FLS980 fluorescence spectrometer with TMS300 monochromators and a red cooled detector (Hamamatsu R928P). The standard light source for measuring of PL spectra was a 450 W xenon arc lamp.

The electroluminescent device was fabricated by means of vacuum deposition of organic semiconductor layers and metal electrodes onto pre-cleaned ITO-coated glass substrate under vacuum of 10^{-5} Torr. The device was fabricated through the step-by-step deposition of various functional layers. CuI and 4,7-diphenyl-1,10-phenanthroline (Bphen) compounds were used for the hole- and electron-transporting layers, respectively.[45] A Ca layer topped with aluminum (Al) was used as the cathode. The Bphen is a well-known hole blocking layer and electron transporting material[46] being widely used to promote electron transfer from the Ca:Al cathode to the central emissive layer. The structure of the fabricated device was as follows: ITO/CuI(8nm)/ **4** (40nm)/Bphen(10nm)/Ca(50nm):Al(200nm). The active area of the obtained device was 3x6 mm^2.

Characteristics of the current density-voltage and luminance-voltage dependences were measured with a semiconductor parameter analyzer (HP 4145A) using it in air without passivation immediately after fabrication of the device. The measurement of brightness was performed using a calibrated photodiode. The OLED electroluminescence and PL spectra of the solid films were recorded with an Ocean Optics USB2000 spectrometer.

COMPUTATIONAL DETAILS

The equilibrium structural parameters of the **4** molecule were optimized at the B3LYP/6-31G(d)[47, 48, 49] level of the density functional theory (DFT) with a control of possible symmetry

constraints (S_2 symmetry point group), using the Gaussian 09 software package (Revision C.02).[50] We have also calculated the vibrational frequencies for the studied compound in order to verify determination of the true minimum on potential energy surface (PES). All vibrational frequencies are found to be real, which indicates the location of the sought-for energy minimum. The electronic absorption spectra of **4** were calculated by the time dependent (TD) DFT[51] using the polarized continuum model (PCM)[52] to model the chlorobenzene medium using the same B3LYP/6-31G(d) approach.

Reorganization energy values for the electron (λ–) and hole (λ+) carriers have been calculated using the following equation being widely used for estimation of the charge transport properties of organic materials:[53, 54, 55]

$$\lambda_{-/+} = (E^{*}_{-/+} - E_{-/+}) + (E^{**}_{-/+} - E_0), \qquad (1)$$

where E_0 is the optimized ground state energy of 4 neutral molecule, E–/+ is the energy of the optimized anionic/cationic species, $E^{**}_{-/+}$ is the energy of the neutral molecule at the anionic/cationic geometry and $E^{*}_{-/+}$ is the energy of the anionic/cationic molecule at the optimized geometry of the neutral species.

All calculations are performed at the PDC supercomputers of the Royal Institute of Technology, Stockholm.

RESULTS AND DISCUSSION

SYNTHESIS AND CHARACTERISATION

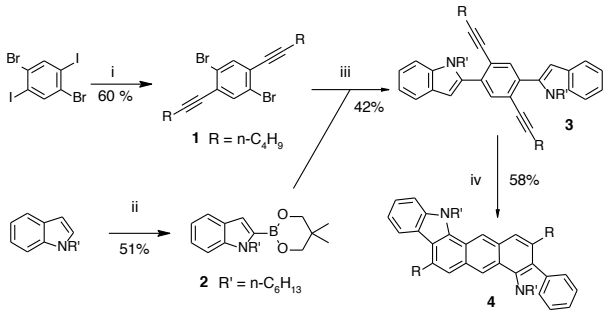

Scheme 1. i.1-hexyne, $PdCl_2(PPh_3)_2$ (12%), CuI (6%) in NEt_3/ DMF (2:1), 20 °C, 86 h; ii. LiTMP, $B(O^iPr)_3$ then $Me_2C(CH_2OH)_2$; iii. $Pd(PPh_3)_4$ (5%), KO^tBu, DMAC, 50-80 °C; iv. DBU, NMP, 202 °C, 3h.

Compound **4** was synthesized in a bidirectional manner from 1,4-dibromo-2,5-diiodobenzene[56] (Scheme 1). Double Sonogashira coupling[57] with 1-hexyne gave bis-alkyne **1** which was elaborated by double Suzuki coupling[56] with the indole boronic ester **2**. The boronic ester was derived by deprotonation of known N-hexylindole[58] with lithium 2,2,6,6-tetramethylpiperidide (LiTMP) with *in-situ* trapping with boron triisopropoxide followed by alcohol exchange with 2,2-dimethyl-propan-1,3-diol**.** A related synthesis of boronated derivatives of N-BOC protected indoles has been reported.[59] However, here the stronger base (LiTMP) was necessary to obtain a good conversion due to the lower acidity of N-alkylindoles. *In situ* transesterification with neopentyl glycol gave cyclic ester **2** which was expected to be more stable against deborylation than the parent boronic acid.

The subsequent Suzuki coupling to obtain **3** was carried out under anhydrous conditions using potassium *t*-butoxide which is a very useful base in the case of boronic derivatives with steric hindrance.[60] Finally base induced double cyclisation of **3** gave the desired bisindoloanthracene **4**.[61, 62] In the realm of organic electronics, base catalysed isomerisation of alkynylated oligomers to polyaromatic semiconductors has been used for the synthesis of coronenes[63, 64, 65, 66] and thienoacenes of various number of rings and sulfur atoms.[67, 68, 69, 70] Here, we demonstrate that this strategy is also suitable for the synthesis of bis-[(1,2)(5,6)]indoloanthracene (**4**) a new π-extended nitrogen based heterocycle.

Compound **4** was obtained as yellow solid possessing fair solubility in chloroform (~5 mg/ml) and a modest solubility in dichloromethane and chlorobenzene. The structure was confirmed by its spectroscopic and analytic data (see Supporting Information). Single crystals suitable for X-ray analysis were obtained by a slow evaporation of a solution on **4** in chloroform/ethyl acetate. X-ray diffraction studies show that molecules of **4** crystallise in one monoclinic unit cell ($P2_1/n$ (No. 14) space group) and its molecular structure in the single crystal is shown in Figure 1a.[71] As can be seen from the Figure 1a a single molecule of **4** possesses a almost planar structure with a condensed

ribbon consisting of pyrrole and benzene rings. Molecules of **4** are packed in the single crystal in a face to face arrangement with only a small percentage of an overlap of the π-frameworks resulting in a slipped face to face packing (Figure 1b). The inter-plane distance of two "sandwiched" molecules of **4** is 3.55Å with the shortest inter atom contact of 3.54 Å (between N1 and the C15'), both being larger than the inter-planar distance in graphite (3.35 Å). Such herring bone packing motif is also observed in some linear N-alkylindolocarbazoles.[10, 13]

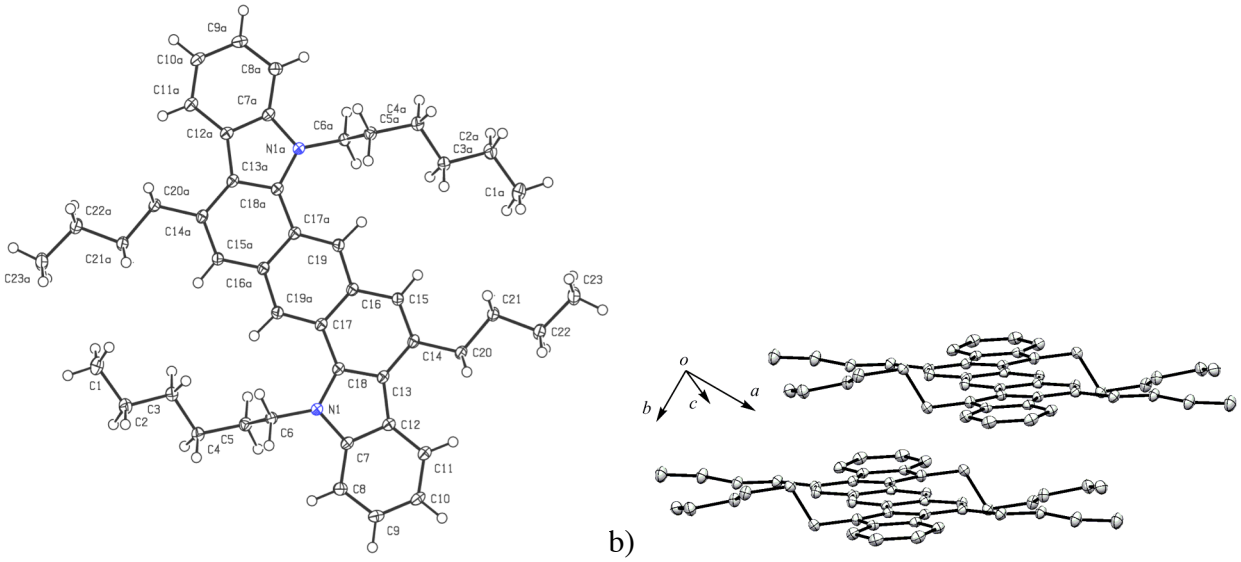

a) b)

Figure 1. X-ray crystal structure (ORTEP) of the single **4** molecule including the atomic numbers (a) and the X-ray crystal packing fragment (b) containing only the two neighboring molecules located at the opposite planes (Hydrogen atoms omitted for clarity). Thermal ellipsoids are drawn at 50% probability. See also Figure S14 for the different views of crystal packing.

A comparison of the DFT calculated and X-ray measured bond lengths for the **4** molecule indicates a good agreement between the theoretical and experimental values (as can be seen from the Table 1 the average bond lengths difference does not exceed 0.01 Å, which validates the choice of the functional and the basis set for the geometry optimization procedure). Despite its extended π-conjugated scaffold **4** shows a remarkable thermal stability up to 390 °C as given the thermal gravimetric analysis (TGA) of the solid material. The weight stays invariant up to 390 °C, suggesting for **4** a long-time thermal stability under ambient conditions and being suitable for vacuum deposition processing. The thermal transitions of **4** have been studied by DSC showing a significant melting endotherm (T_m = 212 °C) and the corresponding exotherm crystallization (T_c = 201 °C).

Notably, a second endotherm transition and two minor exotherm transitions were observed that probably describe some disorder created by the two alkyl groups of different chain length. The "alkyl chain melting" transition is observed during the heating and occurs at 152 °C, with two corresponding exotherm transitions at 175 °C and 143 °C during the cooling process (For TGA and DSC, see Supporting Information).

Table 1. The selected bond lengths (Å) for the 4 molecule.

atom	atom	X-ray	B3LYP/ 6-31G(d)	atom	atom	X-ray	B3LYP/ 6-31G(d)
N1	C7	1.3862(17)	1.388	C13	C14	1.434(2)	1.434
N1	C18	1.3927(18)	1.397	C13	C18	1.4028(19)	1.412
C7	C8	1.401(2)	1.401	C14	C15	1.3652(19)	1.370
C7	C12	1.414(2)	1.420	C15	C16	1.4391(19)	1.430
C8	C9	1.383(2)	1.390	C16	C17	1.438(2)	1.445
C9	C10	1.404(2)	1.406	C16	C19	1.4036(19)	1.402
C10	C11	1.385(2)	1.390	C17	C18	1.4418(19)	1.441
C11	C12	1.4082(19)	1.407	C17	C19a	1.4044(19)	1.402
C12	C13	1.4478(19)	1.445	N1	C6	1.4603(18)	1.459

a=-x, -y, -z Only half of bond lengths are given in Table 1 since the molecule possesses the S_2 symmetry point group. All the C–C bonds in the benzene rings demonstrate the aromatic nature with bond lengths at about 1.4 Å.

With the aim to investigate the redox potential levels and to estimate HOMO/LUMO energies, cyclic voltammetry was carried out in the presence of Bu_4NPF_6 (0.1 M in CH_2Cl_2) with Fc^*/Fc^{*+} (-0.13 V vs SCE[72]) as internal standard. Two quasi-reversible oxidation waves were found for **4** at $E^{ox}_{1/2}$ (I) = 0.67 V and $E^{ox}_{1/2}$ (II) = 1.09 V, respectively (Figure 2). From the onset of the first oxidation half-wave E^{ox}_{onset} (I) = 0.59 V, the HOMO energy level of **4** was estimated to E(HOMO) = -5.23 eV with $E_{HOMO} = -(E_{onset} - 0.46_{\text{for Fc+/Fc vs SCE}} + 5.10)$ (eV) for measurements in CH_2Cl_2 solution (0.1M Bu_4NPF_6 as supporting electrolyte). Based on a recent discussion of G.C. Bazan *et al.* we choose here -5.10 eV as the formal potential of the Fc^+/Fc redox couple in the Fermi scale and not the quite often used value of -4.8 eV for 0.0 V versus Fc^+/Fc.[73] The former calibration scale of -

5.10 eV is based on a set of empirically obtained electrochemical data and reflects best the stability of the redox species involved.

Such a low level HOMO characterizes **4** as being suitable for both hole injection as well as hole transport and furthermore should guarantee a reasonable long term stability. The energy level of the lowest unoccupied molecular orbital (LUMO) was estimated by adding the value of the optical band gap taken from the onset of the absorption spectra of **4** in CH_2Cl_2 (λ_{onset} = 450 nm, 2.76 eV) providing E_{LUMO} = -2.76 eV. The DTF calculated energy of the HOMO and LUMO orbitals (Table 2) are overestimated comparing with the experimental electrochemical measurements as expected.[74] Here, one has to consider that the experimentally obtained formal potentials reflect relative stabilities of the involved redox species which can be correlated to HOMO/LUMO energy levels and should follow the same trend, but always will be obtained with error margins depending on the chosen calibration scale. However both theoretical and experimental results qualitatively agree that **4** represents a wide-bandgap semiconducting material.

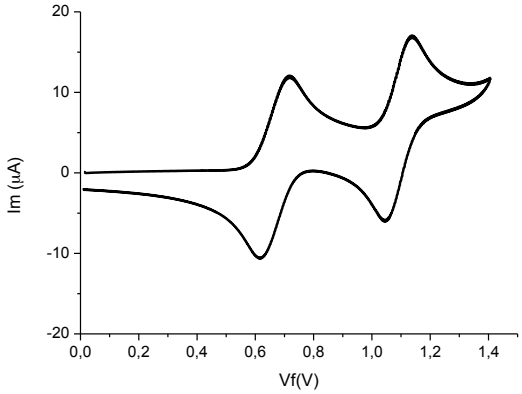

Figure 2. Cyclic voltammetry of **4** ($6x10^{-4}$ M in CH_2Cl_2 / 0.1 M Bu_4NPF_6) at room temperature. Scan rate 200 mV/s, values corrected vs. internal Fc* (-0.13 V vs SCE).

Table 2. Energies of frontier molecular orbitals of 4, calculated by DFT B3LYP/6-31G(d) method and determined by cyclic voltammetry and UV-vis spectroscopy.

data	E_{HOMO} (eV)	E_{LUMO} (eV)	HOMO/LUMO Gap (eV)
experimental	-5.23	-2.47	2.76

calculated	-4.74	-1.48	3.28

The shapes of the HOMO and LUMO orbitals for bis-indoloanthracene **4** are presented in Figure 3. As can be seen from Figure 3 both orbitals represent the π-type wave-functions localized predominantly on the central anthracene unit with only minor contributions from the indole moieties. Moreover both HOMO and LUMO orbitals of **4** are closely similar to the well known b_{2g} HOMO and b_{3u} LUMO frontier molecular orbitals of the parent anthracene molecule (D_{2h} point group).[75] They also belong to *gerade* and *ungerade* symmetries and are concentrated near the inversion center. Thus, it is logical to observe some similarity in the electronic absorption and emission spectra of **4** in comparison to the parent anthracene, though the positions and relative intensities of the band maxima are rather different.

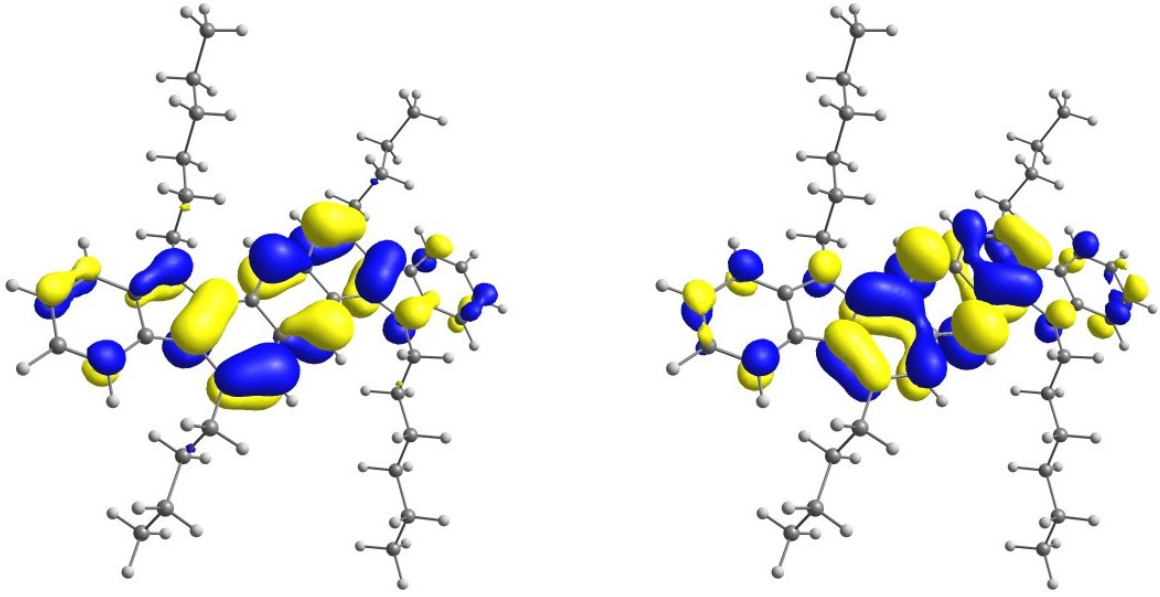

a) b)

Figure 3. Frontier molecular orbitals of **4** calculated with the B3LYP/6-31G(d) method. a) HOMO, b) LUMO.

The ionization potential (I_p) of the solid films of **4** was estimated from electron photoemission spectra, which are presented in Figure 4. The high I_p value (5.16 eV) of **4** is in agreement with the electrochemistry data (E_{HOMO} = -5.23 eV) and will facilitate hole injection from the anode into the organic layer, as well as charge transport of injected holes to the emitting layer in OLEDs.[76]

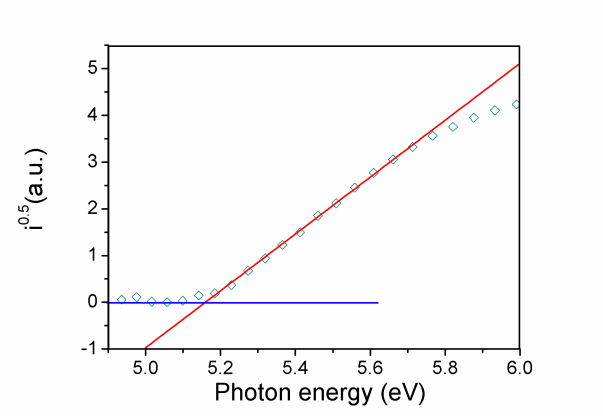

Figure 4. Photoelectron emission spectra of the solid state films of **4**.

With the aim to design an OLED where **4** will function as the emitting layer the charge transport properties of films of **4** were investigated by the use of the time of flight (TOF) method under ambient conditions. Understanding the transport properties of the emissive layers is necessary to design a particular OLED architecture.[77] A higher mobility through the emissive layer provides a wider recombination zone, which is found to be responsible for longer OLED lifetimes and lower drive voltage at the expense of luminance yield.[78] Solid films of **4** indicate the hole mobility equal to $\mu = 10^{-3}$ cm^2 V^{-1} s^{-1} (Figure 5a). Such a hole mobility allows **4** to be used as the hole-transport layer on par with traditional hole-transporting materials like *N*,*N*'-bis(naphthalen-1-yl)-*N*,*N*'-bis(phenyl)-benzidine (α-NPD) and *N*,*N*'-bis(3-methylphenyl)-*N*,*N*'-diphenyl-[1,1'-biphenyl]-4,4'-diamine (TPD).[79, 80] DFT predictions for the charge carrier mobility of **4** confirm good hole-transporting properties together with electron-transporting possibility. The calculated values of the hole and electron reorganization energies (λ_+ and λ_-, respectively) both are equal to 191 meV which usually corresponds to $\mu = 10^{-3} - 10^{-2}$ cm^2 V^{-1} s^{-1} for ambipolar semiconductors (in the framework of Marcus theory).[81] These theoretical predictions are in good agreement with the above TOF experiment.

The experimental data of Figure 5a are well described by the equation $\mu = \mu_0 \cdot exp(a \cdot E^{1/2})$ for external electric field E > 0.4 × 10^5 V·cm^{-1} (E$^{1/2}$> 200 (V·cm^{-1})$^{1/2}$), where μ_0 is determined as the zero field electron mobility and a is the field enhancement factor of the Poole–Frenkel type mobility.

To calculate the hole mobility of **4** the following equation $\mu = d^2/U \cdot t_{tr}$ was used, where d is the film thickness, t_{tr} is the transit time, and U is the applied voltage; the transit times were determined from

the intersection of the asymptotes to the plateau and the tail of the transient signal in double logarithmic plots (Figure 5b). As illustrated in Figure 5b (insert), the tails of the photocurrent transients of **4** are far more dispersive, indicating the dispersive hole transport of the **4** film.

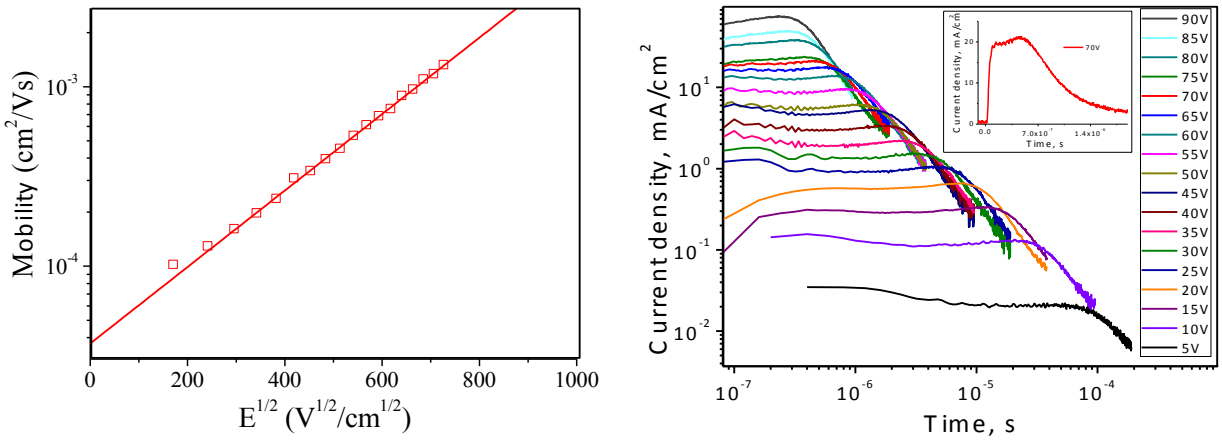

a) b)

Figure 5. Electric field dependencies of the hole-drift mobility of **4** compound measured by TOF methods (a) and current transient pulses of **4** compound with different electric fields (b) at room temperature.

A distinctive plateau is visible in the TOF transient of the **4** compound in liner plots, which indicates the non-dispersive hole transport (Figure 5b, insert). This fact corresponds to the small density of shallow charge traps because of the high film ordering.[82] Indeed, the X-ray powder diffraction (XRD) measurement attests the presence of an ordered structure for the **4** solid sample (Figure 6).

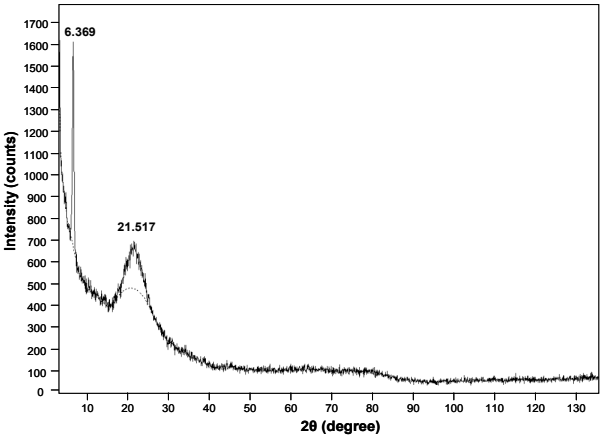

Figure 6. X-ray diffraction pattern of the **4** powder.

In particular we observe a narrow high-intensity signal at 2θ = 6.369° which corresponds to the long-range order of **4** in its crystal structure with a very high inter-plane distance of 13.87 Å as calculated using Bragg's law. The next broad reflex at about 2θ = 21.517° indicates the presence of dispersed crystal grains of **4** with an average inter-plane distance of 4.13 Å. This value can be attributed to the intermolecular distance between the two planes of neighboring **4** molecules. Indeed the value of 4.13 Å is in a good agreement with the more precise data for the single crystal of **4** where the interplane distance was found to be equal to 3.55 Å and taking into account the broad nature of the corresponding XRD reflex.

OPTICAL AND PHOTOPHYSICAL PROPERTIES

The absorption spectra of **4** measured in solution and thin film are presented in Figure 7 together with the TD DFT simulated curve (band half-width is 2500 cm^{-1}). The TD-DFT/B3LYP/6-31G(d) simulations allow the assignment of the observed maxima as summarized in Table 3. The absorption spectrum of the solid film of **4** undergoes spectral broadening and a "red" shift of absorption peaks relative to the absorption spectrum of **4** in chlorobenzene solution (Figure 7). These effects can be associated with the presence of aggregated **4** having a partly "plane-to-plane" or π-stacked type coupling (Figure S17, S18).[83, 84] However, it is assumed that the film has not a fully periodical or hierarchical structure and might be understood as a containing at least two chromophores originated from the same molecule. The later might be reasoned by the red-shift, broadening and intensity changes observed between the spectra in solution and solid state film (see also discussion below and Figure 8).

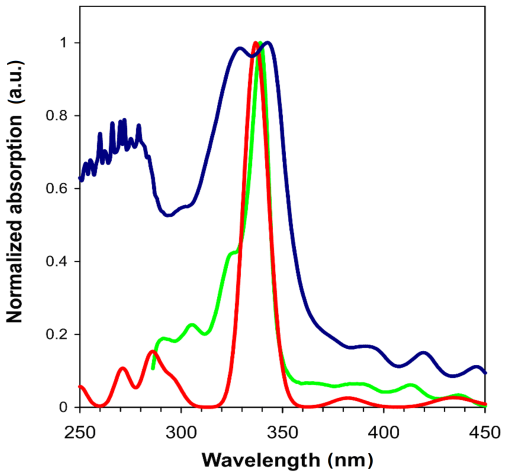

Figure 7. UV-Vis absorption spectra of **4** compound measured in chlorobenzene (green line) and for the solid state film (blue line) together with the D-DFT/B3LYP/6-31G(d) simulated curve (red line) accounting the PCM approach.

The first absorption band calculated at 435 nm corresponds to the transition into the S_1 excited state which consists of the single HOMO-LUMO configuration. This band is similar by the orbital nature to the *p*-band of anthracene observed at 368 nm in its absorption spectrum measured in an argon matrix.[85] This band produces the clear-cut vibronic progression in both solution and solid-state absorption and emission spectra of **4** with the same (approximately) vibronic spacing equal to 1277 and 1338 cm^{-1}, respectively (Figure 8).

The second and third absorption bands can be assigned as the α- and β-bands by analogy to the anthracene spectrum accounting that the λ_α band is almost forbidden and overlapped by the λ_P band in the spectrum of the parent anthracene. This is in contrast to the absorption spectra of **4** for which the λ_α band is clearly separated (Figure 7, Table 3). The corresponding S_2 and S_4 excited states are formed both by HOMO □ LUMO+1 and HOMO−1 □ LUMO configuration with the opposite signs and weight (Table 3).

Table 3. Calculated Energy (λ), Oscillator Strength (*f*) and Orbital Assignment of the singlet-singlet vertical electronic transitions for compound 4.

State	λ,[a] nm	λ_{exp},[b] nm	*f*	Orbital Assignment
S_1	435	436, (413)	0.065	λ_P: HOMO □ LUMO (98%)
S_2	382	388 (365)	0.063	λ_α: (+) HOMO □ LUMO+1 (65%) (+) HOMO–1 □ LUMO (32%)
S_4	337	339 (324) [305]	2.465	λ_β: (+) HOMO–1 □ LUMO (66%) (–) HOMO □ LUMO+1 (31%)

[a] calculated value; [b]chlorobenzene solution. The numbers in parentheses and in brackets correspond to the 0-1 and 0-2 vibronic satellites, respectively taken from the experimental spectra in solution.

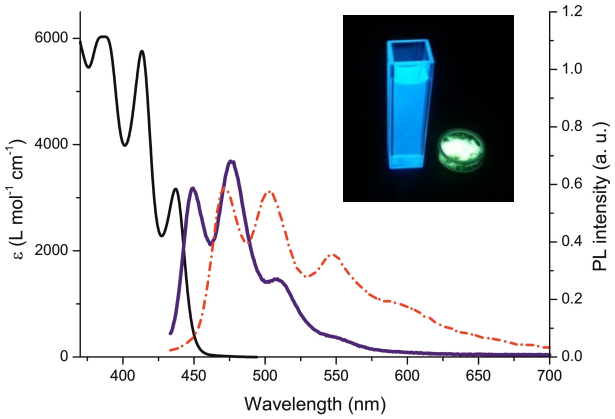

Fig 8. Absorption (black) and emission spectra (λ_{ex} = 390 nm) of **4** in chlorobenzene (1.4 x 10^{-5} M, blue), and of crystalline **4** (red). Insert, PL of **4** in solution and from crystals.

The solid state (crystals) and solution phase emission spectra of compound **4** are shown in Figure 8 together with the UV-absorption in chlorobenzene. The photoluminescence spectrum of **4** in solution is characterized by three intense maxima at 449 nm, 478 nm, and 509 nm respectively (Table 4), as well as a broad shoulder at 552 nm. The corresponding, and significantly red-shifted, bands can be found in the solid state emission spectra of **4** at 472 nm, 503 nm, and 548 nm, respectively with a broad shoulder at 600 nm. The three main photoluminescence bands are identified as vibronic sequence (0-0 band 449 nm, 0-1 band 478 nm and 0-2 band 509 nm, for solution spectra). The same assignment can be made for the emission maxima in the solid state spectra that is red-shifted due to aggregated **4** in the crystals. Notably, the observation of a structured luminescence spectra of **4** in the solid state being quite similar to the vibronic sequence in solution evidently indicates that the observed bathochromic shift from solution to solid state

emission is due to an aggregate effect and not to excimer emission of **4**. The maxima as well as the relative band intensities are clearly different for both spectra because the stacking aggregation phenomenon affects the vibronic transition probability through the change of transition dipole moment between corresponding vibrational functions.[86, 87] Indeed, the Franck-Condon factors in a tight-bound packing can differ from those of a free molecule because of different displacements of potential energy surfaces in the ground and excited states.

Table 4. Comparison of photoluminescence spectra of **4** in solution (chlorobenzene), crystals and solid film (vacuum deposited).

4	λ^{F}_{max} (1)	λ^{F}_{max} (2)	λ^{F}_{max} (3)	λ^{F}_{sh} (4)
Solution	449	478	509	550
Crystals	472	503	548	600
Solid Film	450	484	520	560

Notably, the photoluminescence spectrum of vacuum deposited **4** is quite related to the solution spectra with slightly red-shifted maxima and changes within the relative emission intensities (Figure 9). The thin film spectra can be interpreted as a superimposition of the solution and the solid state emission spectra - or in other words it shows the presence of two emitters in a single emissive region through the formation of stacked aggregates by one of the emitting species. Therefore, the vacuum deposited thin-film of **4** can be regarded as a combination of an amorphous or molecular **4** layer that contains crystalline grains with aggregated **4**. The latter having a similar next order packing as the one found in the single crystal structure.

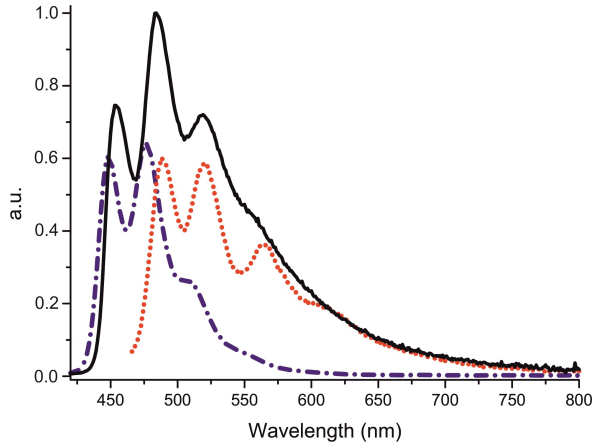

Figure 9. Photoluminescence spectra of **4** of a vacuum deposited layer (black solid line), and in comparison the one in solution (blue line, 1.4 x10^{-5} M in chlorobenzene, λ_{ex} = 390 nm) and of crystals (red dotted line, λ_{ex} = 390 nm).

Solutions of **4** show a bright blue emission with high quantum yields ($\theta_F^{solution}$ = 68%, λ_{ex} = 390 nm, 10^{-6} M in CH_2Cl_2). Whereas the yellow-green emission of crystalline **4** is accompanied by a significantly lower quantum yield (θ_F^{solid} = 22%, λ_{ex} = 420 nm) due to aggregation caused emission quenching effects. The fluorescence decay kinetics of a vacuum deposited film of **4** is presented in Figure 10. The transients follow single recorded rate at photoluminescence band maxima 450, 484 and 520 nm; they exhibit two-exponential decay profile with the decay time constants (τ) of a few nanosecond scale, that can be assigned to the **4** exciton fluorescence.[88, 89] The lower energy emission (560 nm) decays slowly and the character of curves represents the three-exponential functions (Figure 10, Table 5), with longer decay time constants. The non-monoexponential decay profile at 560 nm indicates the presence of different types of excited states: apart from excitons appears the emission from aggregates of **4** with higher photoluminescence lifetimes.[90]

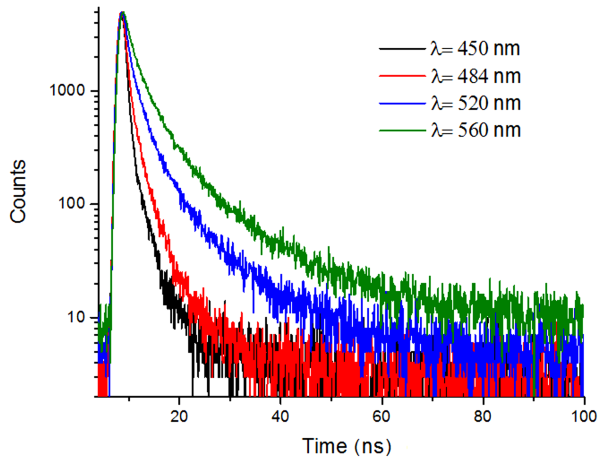

Figure 10. The decay fluorescence of **4** films measured at different wavelengths: 450, 484, 520 and 560 nm.

Table 5. Fitting results of the photoluminescence transients of the 4 solid films prepared by vacuum deposition at 300 K.

Wavelength of PL spectra (nm)	450	484	520	560
Photoluminescence lifetimes (τ) (ns)	0.5 (88%) 2.9 (12%)	0.6 (74%) 3.0 (26%)	1.2 (66%) 6.4 (34%)	0.65 (37%) 2.6 (47%) 10 (16%)
χ^2	1.28	1.44	2.00	1.25

OLED CHARACTERISATION

Electroluminescence (EL) spectrum of the fabricated OLED (Figure 11) is quite similar to the PL spectrum of the vacuum deposited **4** film (Figure 8). The electroluminescence spectrum of the device (ITO/CuI/**4**/Bphen/Ca:Al) shown in Figure 11 is characterized by three emission bands: at 450 nm, 484 nm and 520 nm which corresponds to the **4** exciton emission. The electroluminescence spectrum of the OLED formed from **4** also reflects the emission characteristics of molecular **4** superimposed by emission of crystalline domains with aggregated **4**. The observed discrepancy between the EL and PL spectra could be ascribed to the self-absorption phenomenon which was observed for the other sky-blue emitter.[91]

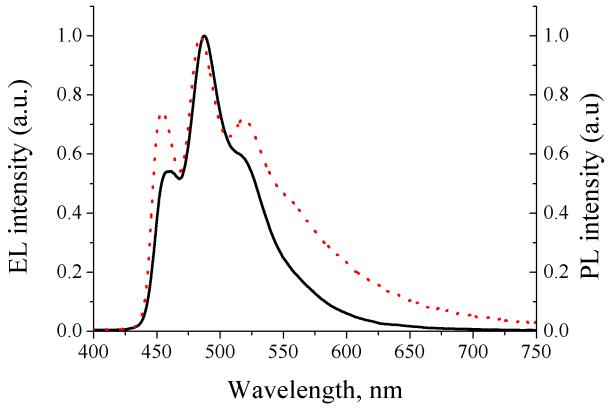

Figure 11. Electroluminescence spectrum of the device ITO/CuI/4/Bphen/Ca:Al (black solid line) and photoluminescence spectra of **4** of a vacuum deposited layer (red dotted line).

Figure 12 shows the current density-voltage characteristics and luminance-voltage characteristics of the electroluminescent device. The designed OLED shows a low turn-on voltage (V_{on}) of 3.6 V for electroluminescence (at 2 cd/m^2). The fabricated device exhibits current efficiency values of 3.5 cd/A and a maximum brightness of 10000 cd/m^2 (at 15 V). Chromaticity coordinates (x, y) of the device are found to be (0.20, 0.31) which corresponds to greenish-blue tint commonly referred to as "sky-blue"color.[92] The external quantum efficiency reaches 1.6 % (Figure 12 c).

The efficiency of the device investigated in this work is achieved due to the high values of photoluminescence quantum yields for solid **4** together with the successful selection of the hole transporting layer, hole blocking layer and electron transporting layer (Figure 13).[93] These materials provide a favorable charge carrier balance at the exciton recombination area. This fact is especially important in the context of the relatively high hole mobility in the emissive layer.

The current efficiency and brightness of the fabricated OLED is quite high compared with solution processed sky blue phosphorescent OLEDs based on iridium complexes, including well known FIrpic.[94] Most of the parameters of **4**-based OLEDs are significantly higher when compared to devices fabricated from asymmetric extended carbazoles, but this observation is countered with deeper/purer blue emission seen for the latter. [39, 41]A quite similar bright blue emission was observed for OLEDs based on trialkylsilylanthracene yet with much lower luminosity of 107 cd/m^2 at 10 V.[91] The sky-blue OLEDs designed from benzo[k]fluoranthene[90] are matching ours

suggesting a great potential in application of the more extended fused polyaromatics. Yet a considerable amount of work is required before such materials will be competetive with the best oligomeric emitters.[95]

Finally, previously fabricated OLEDs based on naphtho[2,3,a]pyrene possess similar technical characteristics compared with the *bis*-[(1,2)(5,6)]indoloanthracene-(**4**)-based device.[96] However, **4** demonstrates a much higher stability than the naphtho[2,3,a]pyrene. Likewise can be stated in comparison with FIrpic which is known to decompose during vacuum processing.[94] Moreover, **4**-based OLEDs are much easier to fabricate as they do not require the use of host materials and precise doping procedures.[90, 97] Hence, angular fused polyaromatic semiconductors may provide interesting alternative to transition metal complexes or oligomers.[98]

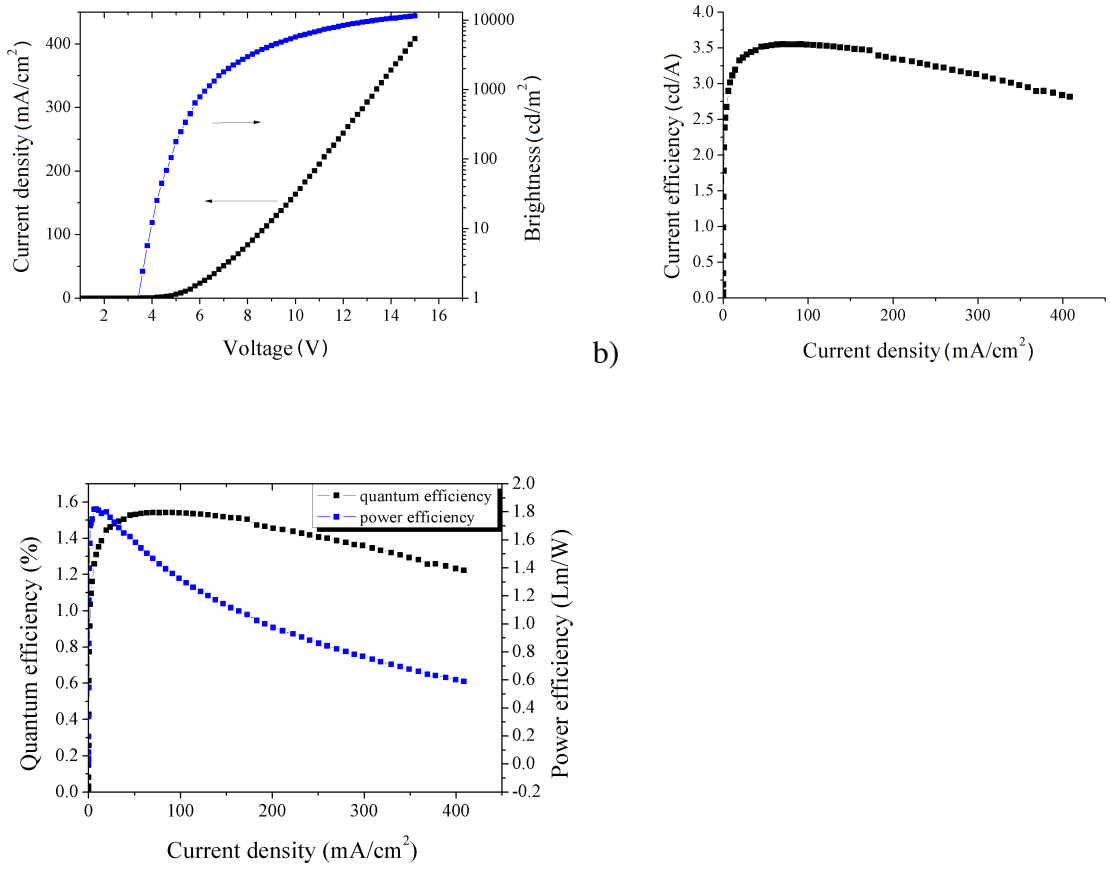

Figure 12. Current density *vs.* voltage, luminance *vs.* voltage characteristics (a), current efficiency *vs.* current density characteristic (b) and Current density *vs.* power and quantum efficiency characteristics (c) of the fabricated OLED from **4**.

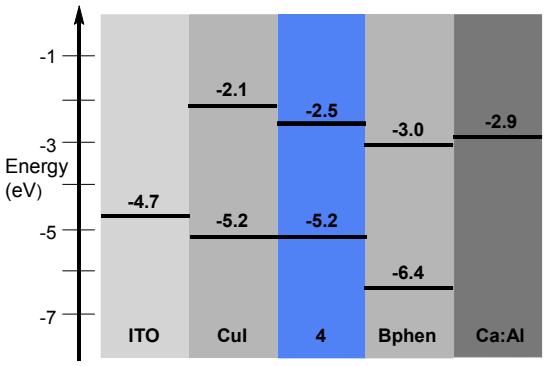

Figure 13. Energy-band diagrams of the fabricated OLED device incorporating *bis*-[(1,2)(5,6)]indoloanthracene-(**4**)**.**

CONCLUSIONS

We report the first synthetic protocol for the novel sky-blue-light emitting *bis*-[(1,2)(5,6)]indoloanthracene (**4**). This compound has been found to be a good hole-transporting material together with possessing high thermal and electrochemical stability. Using **4** as the emissive layer an effective highly luminous OLED sample was fabricated. The obtained device is characterized by a broad electroluminescence spectrum that is achieved from two emitters both originated from **4**. It can be identified as the superimposition of exciton emission and emission components resulting from aggregated **4**. The latter is much more clearly seen in the photoluminescence spectrum of **4** from either crystals or thin film and can be associated with plane-to-plane stacked aggregates as found in the single crystal x-ray structure. Compound **4** is a good hole-transporting material and has high thermal and electrochemical stability. Although this first OLED sample operating with **4** reaches a high luminance of more than 10000 cd/m^2, colour, current efficiencies and external quantum efficiencies need to be improved by fine tuning of the active layer. Importantly, the here reported bidirectional straightforward synthesis of bis-[(1,2)(5,6)]indoloanthracene (**4**) is suitable for obtaining such fine-tuned materials and will allow these future modifications.

Acknowledgments

RJW, BW and PG thank the European Regional Development Fund (ERDF) for funding as part of Interreg IV A project MEET (Materials for Energy Efficiency in Transport). This work was also supported by the Ministry of Education and Science of Ukraine, project no. 0115U003637. G. W-S. acknowledges the financial support of the National Science Centre (Poland) through the Grant No. 2012/04/S/ST4/00128. This research was funded by a grant (No. MTEPI-P-15008) from the R&D and Innovation Fund of Kaunas University of Technology. B. Minaev acknowledges the fellowship of Chinese Academy of Science under the CAS President's International Initiative for Visiting Scientists.

SUPPORTING INFORMATION

Experimental procedures, characterization of data for all new compounds, crystallographic data of **4**, calculations. This material is available free of charge via the Internet at http://pubs.acs.org.

CORRESPONDING AUTHOR

* bernhard.witulski@ensicaen.fr; +33 (0)231 45 2885

** rjw1@soton.ac.uk; +44(023) 8059 2777

NOTES

The authors declare no competing financial interest.

REFERENCES

1 Arbaciauskiene, E.; Kazlauskas, K.; Miasojedovas, A.; Jursenas, S.; Jankauskas, V.; Holzer, W.; Getautis, V.; Sackus, A. Multifunctional Polyconjugated Molecules with Carbazolyl and Pyrazolyl Moieties for Optoelectronic Applications. *Synth. Met.* **2010**, *160*, 490–498.

2 Yang, X.; Xu, X.; Zhou, G. Recent Advances of the Emitters for High Performance Deep-Blue Organic Light-Emitting Diodes. *J. Mater. Chem. C.* **2015**, *3*, 913–944.

3 Sekine, C.; Tsubata, Y.; Yamada, T.; Kitano, M.; Doi, S. Recent Progress of High Performance Polymer OLED and OPV Materials for Organic Printed Electronics. *Sci. Technol. Adv. Mater.* **2014**, *15*, 034203.

4 Minaev, B.; Baryshnikov, G.; Ågren, H. Principles of Phosphorescent Organic Light Emitting Devices. *Phys. Chem. Chem. Phys.* **2014**, *16*, 1719−1758.

5 Guo, X.; Baumgarten, M.; Müllen, K. Designing π-Conjugated Polymers for Organic Electronics. *Progress in Polymer Science*. **2013**, *38*, 1832–1908.

6 Kato, S.-I.; Furuya, T.; Nitani, M.; Hasebe, N.; Ie, Y.; Aso, Y.; Yoshihara, T.; Tobita, S.; Nakamura, Y. A Series of π-Extended Thiadiazoles Fused with Electron-Donating Heteroaromatic Moieties: Synthesis, Properties, and Polymorphic Crystals. *J. Org. Chem.* **2012**, *77*, 7595–7606.

7 Parkhurst, R. R.; Swager. T. M. Synthesis and Optical Properties of Phenylene-Containing Oligoacenes. *J. Am. Chem. Soc.* **2012**, *134*, 15351–15356.

8 Xu, C.; Wakamiya, A.; Yamaguchi, S. Ladder Oligo(*p*-phenylenevinylene)s with Silicon and Carbon Bridges. *J. Am. Chem. Soc*. **2005**, *127*, 1638–1639.

9 Wu, Y.; Li, Y.; Gardner, S.; Ong, B. S. Indolo[3,2-*b*]carbazole-Based Thin-Film Transistors with High Mobility and Stability. *J. Am. Chem. Soc.* **2005**, *127*, 614–618.

10 Reig, M.; Puigdollers, J.; Velasco, D. Molecular Order of Air-Stable p-Type Organic Thin-Film Transistors by Tuning the Extension of the π-Conjugated Core: the Cases of Indolo[3,2-*b*]carbazole and Triindole Semiconductors. *J. Mater. Chem. C*. **2015**, *3*, 506–513.

11 Wakim, S.; Bouchard, J.; Simard, M.; Drolet, N.; Tao, Y.; Leclerc, M. Organic Microelectronics: Design, Synthesis, and Characterization of 6,12-Dimethylindolo[3,2-*b*]carbazoles. *Chem. Mater*. **2004**, *16*, 4386–4388.

12 Ting, H.-C.; Chen, Y.-M.; You, H.-W.; Hung, W.-Y.; Lin, S.-H.; Chaskar, A.; Chou, S.-H.; Chi, Y.; Liu, R.-H.; Wong, K.-T. Indolo[3,2-*b*]carbazole/benzimidazole Hybrid Bipolar Host Materials for Highly Efficient Red, Yellow, and Green Phosphorescent Organic Light Emitting Diodes. *J. Mater. Chem*. **2012**, *22*, 8399–8407.

13 Boudreault, P.-L. T.; Wakim, S.; Blouin, N.; Simard, M.; Tessier, C.; Tao, Y.; Leclerc, M. Synthesis, Characterization, and Application of Indolo[3,2-*b*]carbazole Semiconductors. *J. Am. Chem. Soc*. **2007**, *129*, 9125-9136.

14 Boudreault, P.-L. T.; Wakim, S.; Tang, M. L.; Tao, Y.; Bao, Z.; Leclerc, M. New Indolo[3,2-*b*]carbazole Derivatives for Field-Effect Transistor Applications. *J. Mater. Chem*. **2009**, *19*, 2921–2928.

15 Liu, Z.; Cao, D.; Chen, Y.; Fang, Q. TPA-active D–π–D Fluorophores with Rigid, Planar Cores from Phenylene to Indenofluorene and Indolocarbazole. *Dyes Pigm*. **2010**, *86*, 63–67.

16 Lin, X.; Tani, Y.; Kanda, R.; Nakayama, K.; Yagai, S. Indolocarbazoles End-Capped with Diketopyrrolopyrroles: Impact of Regioisomerism on the Solid-State Properties and the Performance of Solution-Processed Bulk Heterojunction Solar Cells. *J. Mater. Chem. A*. **2013**, *1*, 14686–14691.

17 Belletete, M.; Boudreault, P.-L. T.; Leclerc, M.; Durocher, G. Structural, Electronic, and Optical Properties of Novel Indolocarbazole-Based Conjugated Derivatives. *J. Mol. Struct: THEOCHEM*. **2010**, *962*, 33–37.

18 Boudreault, P.-L. T.; Virkar, A. A.; Bao, Z.; Leclerc, M. Synthesis and Characterization of Soluble Indolo[3,2-*b*]carbazole Derivatives for Organic Field-Effect Transistors. *Org. Electron*. **2010**, *11*, 1649–1659.

19 Li, Y.; Wu, Y.; Ong, B. S. Polyindolo[3,2-*b*]carbazoles: A New Class of p-Channel Semiconductor Polymers for Organic Thin-Film Transistors. *Macromolecules*. **2006**, *39*, 6521–6527.

20 Blouin, N.; Michaud, A.; Wakim, S.; Boudreault, P.-L. T.; Leclerc, M.; Vercelli, B.; Zecchin, S.; Zotti, G. Optical, Electrochemical, Magnetic, and Conductive Properties of New Polyindolocarbazoles and Polydiindolocarbazoles. *Macromol. Chem. Phys*. **2006**, *207*, 166–174.

21 Tsai, J.-H.; Chueh, C.-C.; Lai, M.-H.; Wang, C.-F.; Chen, W.-C.; Ko, B.-T.; Ting, C. Synthesis of New Indolocarbazole-Acceptor Alternating Conjugated Copolymers and Their Applications to Thin Film Transistors and Photovoltaic Cells. *Macromolecules*. **2009**, *42*, 1897–1905.

22 Sprick, R. S.; Hoyos, M.; Wrackmeyer, M. S.; Parry, A. V. S.; Grace, I. M.; Lambert, C.; Navarro, O.; Turner, M. L. Extended Conjugation in Poly(triarylamine)s: Synthesis, Structure and Impact on Field-Effect Mobility. *J. Mater. Chem. C*. **2014**, *2*, 6520–6528.

23 Lu, J.; Liang, F.; Drolet, N.; Ding, J.; Tao, Y.; Movileanu, R. Crystalline Low Band-Gap Alternating Indolocarbazole and Benzothiadiazole-Cored Oligothiophene Copolymer for Organic Solar Cell Applications. *Chem. Commun*. **2008**, 5315–5317.

24 Boudreault, P.-L. T.; Najari, A.; Leclerc, M. Processable Low-Bandgap Polymers for Photovoltaic Applications. *Chem. Mater*. **2011**, *23*, 456–469.

25 Peng, Q.; Liu, X.; Qin, Y.; Xu, J.; Li, M.; Dai, L. Pyrazino[2,3-*g*]quinoxaline-Based Conjugated Copolymers with Indolocarbazole Coplanar Moieties Designed for Efficient Photovoltaic Applications. *J. Mater. Chem*. **2011**, *21*, 7714–7722.

26 Zhou, E.; Cong, J.; Yamakawa, S.; Wei, Q.; Nakamura, M.; Tajima, K.; Yang, C.; Hashimoto, K. Synthesis of Thieno[3,4-*b*]pyrazine-Based and 2,1,3-Benzothiadiazole-Based Donor−Acceptor Copolymers and their Application in Photovoltaic Devices. *Macromolecules*. **2010**, *43*, 2873–2879.

27 Zhang, B.; Yu, L.; Fan, L.; Wang, N.; Hu, L.; Yang, W. Indolo[3,2-*b*]carbazole and Benzofurazan Based Narrow Band-Gap Polymers for Photovoltaic Cells. *New J. Chem*. **2014**, *38*, 4587–4593.

28 Chan, L.-H.; Lin, L.-C.; Yao, C.-H.; Liu, Y.-R.; Jiang, Z.-J.; Cho, T.-Y. Synthesis of Indolo[3,2-*b*]carbazole-Based Random Copolymers for Polymer Solar Cell Applications. *Thin Solid Films*. **2013**, *544*, 386–391.

29 Wakim, S.; Bouchard, J.; Blouin, N.; Michaud, A.; Leclerc, M. Synthesis of Diindolocarbazoles by Ullmann Reaction: A Rapid Route to Ladder Oligo(p-aniline)s. *Org. Lett*. **2004**, *6*, 3413–3416.

30 Levesque, I.; Bertrand, P.-O.; Blouin, N.; Leclerc, M.; Zecchin, S.; Zotti, G.; Ratcliffe, C. I.; Klug, D. D.; Gao, X.; Gao, F. et al. Synthesis and Thermoelectric Properties of Polycarbazole, Polyindolocarbazole, and Polydiindolocarbazole Derivatives. *Chem. Mater*. **2007**, *19*, 2128–2138.

31 Gao, P.; Feng, X.; Yang, X.; Enkelmann, V.; Baumgarten, M.; Mullen, K. Conjugated Ladder-Type Heteroacenes Bearing Pyrrole and Thiophene Ring Units: Facile Synthesis and Characterization. *J. Org. Chem*. **2008**, *73*, 9207–9213.

32 Wang, C.; Nishida, J.; Bryce, M. R.; Yamashita, Y. Synthesis, Characterization, and OFET and OLED Properties of π-Extended Ladder-Type Heteroacenes Based on Indolodibenzothiophene. *Bull. Chem. Soc. Jpn*. **2012**, *85*, 136–143.

33 Park, K. S.; Salunkhe, S. M.; Lim, I.; Cho, C.-G.; Han, S.-H.; Sung, M. M. High-Performance Air-Stable Single-Crystal Organic Nanowires Based on a New Indolocarbazole Derivative for Field-Effect Transistors. *Adv. Mater*. **2013**, *25*, 3351–3356.

34 Park, J. H.; Lee, H. S.; Park, S.; Min, S.-W.; Yi, Y.; Cho, C.-G.; Han, J.; Kim, T. W.; Im, S. Photo-Stable Organic Thin-Film Transistor Utilizing a New Indolocarbazole Derivative for Image Pixel and Logic Applications. *Adv. Funct. Mater*. **2014**, *24*, 1109–1116.

35 Lee, J.; Hwang, H.; Min, S.-W.; Shin, J. M.; Kim, J. S.; Jeon, P. J.; Lee, H. S.; Im, S. Simultaneous Protection of Organic p- and n-Channels in Complementary Inverter from Aging and Bias-Stress by DNA-Base Guanine/Al_2O_3 Double Layer. *ACS Appl. Mater. Interfaces*. **2015**, *7*, 1765−1771.

36 Más-Montoya, M.; Ortiz, R.P.; Curiel, D.; Espinosa, A.; Allain, M.; Facchetti, A.; Marks, T. J. Isomeric carbazolocarbazoles: synthesis, characterization and comparative study in Organic Field Effect Transistors. *J. Mater. Chem. C*, **2013**,*1*, 1959-1969.

37 Zhao, Z.; Wang, Z.; Zhang, X.; Gao, S.; Yang, X.; Duan, X.; Gao, X. Carbazolo[2,1-a]carbazole Diimide: A Building Block for Organic Electronic Materials. *ChemPlusChem*, **2015**, *80*, 57-61.

38 Levick, M. T.; Grace, I.; Dai, S.-D.; Kasch, N.; Muryn, C.; Lambert, C.; Turner, M. L.; Procter, D. J. A Sm(II)-Mediated Cascade Approach to Dibenzoindolo[3,2-b]carbazoles: Synthesis and Evaluation. *Org. Lett.*, **2014**, *16*, 2292−2295.

39 Shi, L.; Liu, Z.; Dong, G.; Duan, L.; Qiu, Y.; Jia, J.; Guo, W.; Zhao, D.; Cui, D.; Tao X. Synthesis, Structure, Properties, and Application of a Carbazole-Based Diaza[7]helicene in a Deep-Blue-Emitting OLED. *Chem Eur. J.* **2012**, *18*, 8092–8099.

40 Curiel, D.; Más-Montoya, M.; Chang, C.-H.; Chen, P.-Y.; Tai, C.-W.; Tárraga, A. Multifunctional Carbazolocarbazoles as Hole Transporting and Emitting Host Materials in Red Phosphorescent OLEDs *J. Mater. Chem. C*, **2013**,*1*, 3421-3429.

41 Hua, W.; Liu, Z.; Duan, L.; Dong, G.; Qiu, Y.; Zhang, B.; Cui, D.; Tao, X.; Cheng N.; Liuc, Y. Deep-Blue Electroluminescence From Nondoped and Doped Organic Light-Emitting Diodes (OLEDs) Based on a New Monoaza[6]helicene *RSC Adv.*, **2015**, *5*, 75–84.

42 Curiel, D.; Más-Montoya, M.; Hummert, M.; Riede, M.; Leo, K. Doped-Carbazolocarbazoles as Hole Transporting Materials in Small Molecule Solar Cells with Different Architectures. *Org. Electron.*, **2015**, *17*, 28-32.

43 Lim, I.; Kim, E.-K.; Patil, S. A.; Ahn, D. Y.; Lee, W.; Shrestha, N.K.; Lee, J.K.; Seok, W.K.; Cho, C.-G.; Han, S.-H. Indolocarbazole Based Small Molecule: an Efficient Hole Transporting Material for Perovskite Solar Cells, *RSC Adv.*, **2015**, *5*, 55321-55327.

44 Miyamoto, E.; Yamaguchi, Y.; Yokoyama, M. Ionization Potential of Organic Pigment Film by Atmospheric Photoelectron Emission Analysis. *Electrophotography*. **1989**, *28*, 364–370.

45 Stakhira, P.; Cherpak, V.; Volynyuk, D.; Ivastchyshyn, F.; Hotra, Z.; Tataryn, V.; Luka, G. Characteristics of Organic Light Emitting Diodes with Copper Iodide as Injection Layer. *Thin Solid Films*. **2010**, *518*, 7016–7018.

46 Khan, M. A.; Xu, W.; Wei, F.; Bai, Y.; Jiang, X. Y.; Zhang, Z. L.; Zhu, W. Q. Highly Efficient Organic Electroluminescent Diodes Realized by Efficient Charge Balance with Optimized Electron and Hole Transport Layers. *Solid State Communications*. **2007**, *144*, 343–346.

47 Becke, A. D. Density-Functional Exchange-Energy Approximation with Correct Asymptotic Behavior. *Phys. Rev. A*, **1988**, *38*, 3098–3100.

48 Lee, C.; Yang, W.; Parr R. G. Development of the Colle-Salvetti Correlation-Energy Formula into a Functional of the Electron Density. *Phys. Rev. B*, **1988**, *37*, 785–789.

49 Francl, M. M.; Petro, W. J.; Hehre, W. J.; Binkley, J. S.; Gordon, M. S.; DeFrees, D. J.; Pople, J. A. Self-Consistent Molecular Orbital Methods. XXIII. A Polarization Type Basis Set for Second-Row Elements. *J. Chem. Phys.* **1982**, *77*, 3654–3665.

50 Frisch, M. J.; Trucks, G. W.; Schlegel, H. B.; Scuseria, G. E.; Robb, M. A.; Cheeseman, J. R.; Scalmani, G.; Barone, V.; Mennucci, B.; Petersson, G. A. et. al. Gaussian, Inc., Wallingford CT, **2009**. Gaussian 09, Revision C.02.

51 Runge, E.; Gross E.K.U. Density-Functional Theory for Time-Dependent Systems. *Phys. Rev. Lett.* **1984**, *52*, 997–1000.

52 Miertus, S.; Scrocco, E.; Tomasi, J. Electrostatic Interaction of a Solute with a Continuum. A Direct Utilization of *Ab initio* Molecular Potentials for the Prevision of Solvent Effects. *Chem. Phys.* **1981**, *55*, 117–129.

53 Datta, A.; Mohakud, S.; Pati, S. K. Electron and Hole Mobilities in Polymorphs of Benzene and Naphthalene: Role of Intermolecular Interactions. *J. Chem. Phys.* **2007**, *126*, 144710.

54 Karaush, N.N.; Baryshnikov, G.V.; Minaev, B.F. DFT Characterization of a New Possible Graphene Allotrope. *Chem. Phys. Lett.* 2014, *612*, 229–233.

55 Raghavachari, K.; Binkley, J. S.; Seeger, R.; Pople, J. A. Self-Consistent Molecular Orbital Methods. 20. Basis Set for Correlated Wave-Functions. *J. Chem. Phys.* **1980**, *72*, 650–654.

56 Goldfinger, M. B.; Crawford, K. B.; Swager, T. M. Directed Electrophilic Cyclizations: Efficient Methodology for the Synthesis of Fused Polycyclic Aromatics. *J. Am. Chem. Soc.* **1997**, *119*, 4578-4593.

57 Chanteau, S. H.; Tour, J. M. Synthesis of Anthropomorphic Molecules: The NanoPutians, *J. Org. Chem.*, **2003**, 68, 8750–8766.

58 Qi, T.; Qiu, W.; Liu, Y.; Zhang, H.; Gao, X.; Liu, Y.; Lu, K.; Du, C.; Yu, G.; Zhu, D. Synthesis, Structures, and Properties of Disubstituted Heteroacenes on One Side Containing Both Pyrrole and Thiophene Rings *J. Org. Chem.* **2008**, *73*, 4638–4643.

59 Vazquez, E.; Davies, I.W.; Payack, J.F. A Non-cryogenic Method for the Preparation of 2-(Indolyl) Borates, Silanes, and Silanols *J. Org. Chem.* **2002**, *67*, 7551-7552.

60 Zhang, H.; Chan, K.S. Base Effect on the Cross-Coupling of Bulky Arylboronic Acid with Halopyridines. *Tetrahedron Lett.* **1996**, *37*, 1043–1044.

61 Wang, Y.; Burton, D. J. Site-Specific Preparation of 2-Carboalkoxy-4-Substituted Naphthalenes and 9-Alkylphenanthrenes and Evidence for an Allene Intermediate in the Novel Base-Catalyzed Cyclization of 2-Alkynylbiphenyls *Org. Lett.* **2006**, *8*, 5295-5298.

62 Lim, J. W.; Kim, K. H.; Kim, S. H.; Kim, J. N. Synthesis of 1H-benzo[g]indazole Derivatives: Propargyl–Allenyl Isomerization and 6π-Electrocyclization Involving Two Aromatic π-Bonds. *Tetrahedron* **2014**, *70*, 6831-6840.

63 Rohr, U.; Schlichting, P.; Böhm, A.; Gross, M.; Meerholz, K.; Bräuchle, C.; Müllen, K. Liquid Crystalline Coronene Derivatives with Extraordinary Fluorescence Properties, *Angew. Chem. Int. Ed.* **1998**, *37*, 1434-1437.

64 Rohr, U.; Kohl, C.; Mullen, K.; Craats, A.; Warman, J. Liquid Crystalline Coronene Derivatives *J. Mater. Chem.*, **2001**, *11*, 1789–1799.

65 An, Z.; Yu, J.; Domercq, B.; Jones, S. C.; Barlow, S.; Kippelen, B.; Marder, S. R. Room-Temperature Discotic Liquid-Crystalline Coronene Diimides Exhibiting High Charge-Carrier Mobility in Air. *J. Mater. Chem.*, **2009**, *19*, 6688–6698.

66 Nolde, F.; Pisula, W.; Muller, S.; Kohl, C.; Mullen, K. Synthesis and Self-Organization of Core-Extended Perylene Tetracarboxdiimides with Branched Alkyl Substituents. *Chem. Mater.* **2006**, *18*, 3715-3725.

67 Rieger, R.; Beckmann, D.; Pisula, W.; Kastler, M.; Müllen, K. Tetrathiahexacene as Building Block for Solution-Processable Semiconducting Polymers: Exploring the Monomer Size Limit. *Macromolecules*, **2010**, *43*, 6264–6267.

68 Shao, J.; Zhao, X.; Wang, L.; Tang, Q.; Li, W.; Yu, H.; Tian, H.; Zhang, X.; Geng, Y.; Wang, F. Synthesis and Characterization of π-Extended Thienoacenes with Up to 13 Fused Aromatic Rings *Tetrahedron Lett.*, **2014**, *55*, 5663–5666.

69 Cheng, S.-W.; Chiou, D.-Y.; Lai, Y.-Y.; Yu, R.-H.; Lee, C.-H. Cheng, Y.-J. Synthesis and Molecular Properties of Four Isomeric Dialkylated Angular-Shaped Naphthodithiophenes *Org. Lett.*, **2013**, *15*, 5338–5341.

70 Cheng, S.-W.; Tsai, C.-E.; Liang, W.-W.; Chen, Y.-L.; Cao, F.-Y.; Hsu, C.-S.; Cheng, Y.-J. Angular-Shaped 4,9-Dialkylnaphthodithiophene-Based Donor–Acceptor Copolymers for Efficient Polymer Solar Cells and High-Mobility Field-Effect Transistors. *Macromolecules*, **2015**, *48*, 2030–2038.

71 Data were collected on a Rigaku AFC12 '-circle goniometer equipped with an enhanced sensitivity (HG) Saturn724+ detector mounted at the window of an FR-E+ SuperBright molybdenum (Mo K 1:K 2 = 0.71073A) rotating anode generator with VHF Varimax optics (70μm focus) operating at 2.475kW (45kV, 55mA). Standard data reduction and crystal structure solution and refinement procedures

were followed. **Crystal Data of 4,** $C_{46}H_{56}N_2$ (M= 636.92 g :mol): monoclinic, space group $P2_1/n$ (No. 14), a = 16.397(3) Å, b = 5.5333(8) Å, c = 19.492(4) Å, β = 96.420(4)°, $\alpha = \gamma = 90°$, V = 1757.4(5) Å^3, T = 100(2) K, Z = 2, Z' = 0.5, μ(MoK$_\alpha$) = 0.069 mm^{-1}, Dcalc = 1.204 g/cm^3, 13855 reflections measured (6.522° $\leq 2\Theta \leq$ 54.97°), 4006 unique (R_{int} = 0.0321, R_{sigma} = 0.0345) which were used in all calculations. The final R1 was 0.0525 ($I > 2\sigma(I)$) and wR_2 was 0.1366 (all data). CCDC **1408736** contains the supplementary crystallographic data for this paper. These data can be obtained free of charge from The Cambridge Crystallographic Data Centre via http://www.ccdc.cam.ac.uk/data_request/cif.

72 Connelly, N. G.; Geiger, W. E. Chemical Redox Agents for Organometallic Chemistry. *Chem. Rev.* **1996**, *96*, 877-910.

73 Cardona, C. M.; Li, W.; Kaifer, A. E.; Stockdale, D. Bazan, G. C. Electrochemical Considerations for Determining Absolute Frontier Orbital Energy Levels of Conjugated Polymers for Solar Cell Applications *Adv. Mater.* **2011**, *23*, 2367-2371.

74 Zhang, G.; Musgrave, C. B. Comparison of DFT Methods for Molecular Orbital Eigenvalue Calculations. *J. Phys. Chem. A* **2007**, *111*, 1554-1561.

75 Zilberg, S.; Haas, Y.; Shaik S. Electronic Spectrum of Anthracene: An ab-Initio Molecular Orbital Calculation Combined with a Valence Bond Interpretation. *J. Phys. Chem.* **1995**, *99*, 16558−16565.

76 Shirota Y. in *Organic Electroluminescence*, Ed: Z. Kafafi, Taylor & Francis, New York 2005.

77 Schwartz, G.; Pfeiffer, M.; Reineke, S.; Walzer, K.; Leo, K.; Harvesting Triplet Excitons from Fluorescent Blue Emitters in White Organic Light-Emitting Diodes. *Adv. Mater.* **2007.** *19*, 3672−3676.

78 Culligan, S. W.; Chen, A. C. - A.; Wallace, J. U.; Klubek, K. P.; Tang, C. W.; Chen S. H. Effect of Hole Mobility Through Emissive Layer on Temporal Stability of Blue Organic Light-Emitting Diodes. *Adv. Funct. Mater.* **2006**, *16*, 1481−1487.

79 Van Mensfoort, S. L. M.; Shabro, V.; de Vries, R. J.; Janssen, R. A. J.; Coehoorn R. Hole Transport in the Organic Small Molecule Material α-NPD: Evidence for the Presence of Correlated Disorder. *J. Appl. Phys.* **2010**, *107*, 113710.

80 Stampor W. Electromodulation of Fluorescence in Hole-Transporting Materials (TPD, TAPC) For Organic Light-Emitting Diodes. *Chem. Phys.* **2000**, *256*, 351−362.

81 Tang, X.-D.; Liao, Y.; Gao, H.-Z.; Geng, Y.; Su, Z.-M. Theoretical Study of the Bridging Effect on the Charge Carrier Transport Properties of Cyclooctatetrathiophene and Its Derivatives. *J. Mater. Chem.* **2012**, *22*, 6907−6918.

82 Kreouzis, T.; Bradley, D. D. C.; Campbell, A. J. Hole and Electron Transport in Poly(9,9-Dioctylfluorene) and Poly(9,9-Dioctylfluorene-*co*-Benzothiadiazole). *Proc. SPIE.* **2004**, *5214*, 141−149.

83 Jagtap, S. P.; Mukhopadhyay, S.; Coropceanu, V.; Brizius, G. L.; Bredas, J.-L.; Collard, D. M. Closely stacked oligo(phenyleneethynylene)s: Effect of π-Stacking on the Electronic Properties of Conjugated Chromophores. *J. Am. Chem. Soc.* **2012.** *134*, 7176−7185.

84 Baryshnikov G. V.; Minaev, B. F.; Minaeva, V. A.; Nenajdenko V. G. Single Crystal Architecture and Absorption Spectra of Octathio[8]circulene and Symtetraselenatetrathio[8]circulene: QTAIM and TD-DFT Approach. J. Mol. Model. **2013**, *19*, 4511−4519.

85 Wolf, J.; Hohlneicher G. High-Resolution One- and Two-Photon Spectra of Matrix-Isolated Anthracene. *Chem. Phys.* **1994**, *181*, 185−208.

86 Minaev, B. F.; Knuts, S.; Ågren, H.; Vahtras, O. The Vibronically Induced Phosphorescence in Benzene. *Chem. Phys.* **1993**, *175*, 245−254.

87 Lindgren, M.; Minaev, B.; Glimsdal, E.; Vestberg, R.; Westlund, R.; Malmström, E. Electronic States and Phosphorescence of Dendron Functionalized Platinum(II) Acetylides. *J. Luminesc.* **2007**, *124*, 302−310.

88 Mitani, T.; Yamanaka, T.; Suzui, M.; Horigome, T.; Hayakawa, K.; Yamazaki I. Time-Resolved Synchrotron Spectroscopy of Exciton Fluorescence in Anthracene Single Crystals. *J. Luminesc.* **1988**, *39*, 313−322.

89 Kalinowski, J. Excimers and Exciplexes in Organic Electroluminescence. *Materials Science-Poland*. **2009**, *27*, 735−756.

90 Lee, Y.-H.; Wu, T.-C.; Liaw, C.-W.; Wen, T.-C.; Feng, S.-W.; Lee, J.-J.; Wu, Y.-T.; Guo, T.-F. Non-Doped Active Layer, Benzo[k]fluoranthene-Based Linear Acenes, for Deep Blue- To Green-Emissive Organic Light-Emitting Diodes. *Org. Electron*. **2013**, *14*, 1064−1072.

91 Landis, C.A.; Parkin, S.R., Anthony, J.E., Silylethynylated Anthracene Derivatives for Use in Organic Light-Emitting Diodes, *Jpn. J. Appl. Phys.*, **2005**, *44*, 3921−3922.

92 Goel, A.; Sharma, A.; Rawat, M.; Anand, R. S.; Kant, R.; Synthesis of Fluorescent C2-Bridged Teraryls and Quateraryls for Blue, Sky-Blue, and Green Color Light-Emitting Devices *J. Org. Chem.*, **2014**, *79* , 10873−10880.

93 Yan, F.; Chen, R.; Sun, H.; Sun, X.W. Organic Light-Emitting Diodes with a Spacer Enhanced Exciplex Emission. *Appl. Phys. Lett.* **2014**, *104*, 153302.

94 Example: Kozhevnikov, V. N.; Zheng, Y.; Clough, M.; Al-Attar, H. A.; Griffiths, G. C.; Abdullah, K.; Raisys, S,; Jankus, V.; Bryce, M. R.; Monkman, A. P. Cyclometalated Ir(III) Complexes for High-Efficiency Solution-Processable Blue PhOLEDs., *Chem. Mater.*, **2013**, *25*, 2352-2358.

95 Jeong, H.; Shin, H.; Lee, J.; Kim, B.; Park, Y.-I.; Yook, K.S.; An, B.-K.; Park, J. Recent Progress in the Use of Fluorescent and Phosphorescent Organic Compounds for Organic Light Emitting Diode Lighting *J. Photon. Energy* **2015**, *5*, 057608.

96 Kwon, J.; Hong J.-P.; Lee, W.; Noh, S.; Lee, C.; Lee, S.; Hong J.-I. Naphtho[2,3,a]pyrene as an Efficient Multifunctional Organic Semiconductor for Organic Solar cells, Organic Light-Emitting Diodes, and Organic Thin-Film Transistors. *Org. Electron.* **2010**, *11*, 1103−1110.

97 Xiao, J.; Liu, Z.; Zhang, X.; Wu, W.; Ren, T.; Lv, B.; Jiang, L.; Wang, X.; Chen, H.; Su, W. et. al. Substituent Effects in Twisted Dibenzotetracene Derivatives: Blue Emitting Materials For Organic Light-Emitting Diodes. *Dyes Pigm.* **2015**, *112*, 176−182.

98 Sasabe, H.; Kido J. Multifunctional Materials in High-Performance OLEDs: Challenges for Solid-State Lighting, *Chem. Mater.*, **2011**, *23*, 621−630.

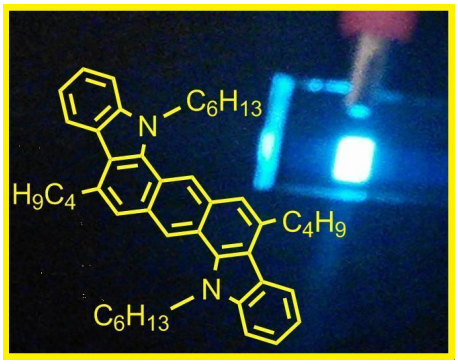
N
C6H13
H9C4
C4H9
N
C6H13